Effect of Dynamic Shear on the Microcellular Foaming of Polypropylene/High-Density Polyethylene Blends

Ping Zhang,[1,2] Xiao-Jun Wang,[3] Yong Yang,[1] Nanqiao Zhou[2]

[1]*College of Electromechanical Engineering, Guang Dong Polytechnic Normal University, Guangzhou, China 510635*
[2]*National Engineering Research Center of Novel Equipment for Polymer Processing, Key Laboratory of Polymer Processing Engineering (Ministry of Education), South China University of Technology, Guanzhou, China 510640*
[3]*Industry College, Jinggangshan University, Ji'an, China 343009*

Received 31 October 2008; accepted 7 April 2009
DOI 10.1002/app.30646
Published online 18 June 2009 in Wiley InterScience (www.interscience.wiley.com).

ABSTRACT: Dynamic shear in the axial direction of a rotor was vertically superposed on the melt flow direction, and its effects on the shear rate and melt strength were investigated theoretically. Polypropylene/high-density polyethylene blends were microcellularly foamed with different vibration parameters. The experimental results were compared with those of a theoretical analysis, and the effects of dynamic shear on the foamability and ultimate cell structure were analyzed in detail. The theoretical results showed that the shear rate and melt strength increased with an increase in the vibration amplitude and frequency. The enhanced melt strength could effectively restrict cell growth, prevent cell rupture, and improve foamability. The experimental results showed that the cell orientation decreased and the cell structure was improved when axial dynamic shear induced by rotor vibrations was superposed on the melt flow direction. Furthermore, the cell diameter decreased and the cell density increased with increases in the vibration amplitude and frequency. The experimental results were very consistent with the theoretical analysis. © 2009 Wiley Periodicals, Inc. J Appl Polym Sci 114: 1320–1328, 2009

Key words: blends; foam extrusion; poly(propylene); (PP)

INTRODUCTION

Polypropylene (PP) has widespread applications in food packaging, cosmetics, and electronics[1] because of its low price, low density, good rigidity, high deformation recovery ratio, super heat and chemical resistance, good degradability, and recyclability. Its field of application will be greatly broadened when PP microcellular foam products are successfully produced for the super properties of microcellular foams. However, PP has very poor foamability because of its high crystallinity and low melt strength, which are due to its linear molecular structure. Therefore, it is very difficult to produce fine PP microcellular foams in experimentation and in industry.

Many new technologies have been used in foaming processes to achieve fine foams, such as the optimization of the die design and the use of the best foaming parameters. Nakajima et al.[2] and Kimura and Nagaoka[3] used a long-land die to produce uniform, crosslinked PP foams. They reported that the foaming agent was heated to its boiling point in the long-land die to provide an expandable resin and produce the uniform expanded article. Baldwin et al.[4] presented a foaming die that could maintain the shaping pressures required to satisfy the shaping and cell growth control requirements. Lee et al.[5] investigated the effects of the variables of the foam extrusion process on the degree of foaming and the growth behavior of gas bubbles. Park et al.[6,7] and Rachtanapapun et al.[8–10] conducted investigations of microcellular foaming for high-density polyethylene (HDPE)/PP blends with batch processing. They reported that the crystallinities of HDPE and PP decreased, the solubility of carbon dioxide (CO_2) in the polymers increased, and the microcellular structure of foamed samples was improved through the blending of PP with HDPE. The relationship of ultrasonic vibrations and microcellular foaming has also been investigated.[11–16] The results show that the cell distribution becomes more uniform and the cell density increases when ultrasonic vibrations are used in the microcellular foaming process. Furthermore, attempts have been made to introduce dynamic shear induced by mechanical vibrations into the microcellular foaming process to improve the fluid shear distribution and cellular structure. The melt shear plays a very important role in the formation of the polymer/gas solution, cell nucleation, and cell growth because the whole

Correspondence to: P. Zhang (cathyzp2002@163.com).
Contract grant sponsor: Foundation of Cultivating Excellent and Innovational Young People of Guangdong Province; contract grant number: LYM08073.

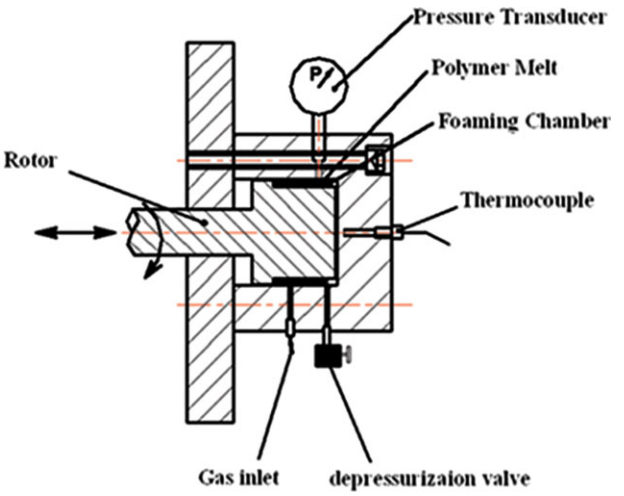

Figure 1 Schematic of the foaming unit of the dynamic simulation foaming setup. [Color figure can be viewed in the online issue, which is available at www.interscience.wiley.com.]

foaming process happens in the polymer melt. Chen et al.[1] reported that the cellular structure was elliptically shaped and that the longer axis of the elliptical cell was aligned along the melt shearing direction when the foaming fluid was mixed in unilateral shear, which led to nonuniformity in each direction for the physical properties of the foam. Dynamic shear was superposed vertically to the flow direction in the foaming process, and its effect on the microcellular foaming process for CO_2/polystyrene blends was investigated by Zhu,[17] Zhou et al.,[18] and Gao and Zhou.[19,20] Their results showed that the mixing performance, gas diffusion rate, and shear rate were enhanced, the formation of the polymer/gas solution was quickened,[19,20] and the nucleation rate increased[17,18] with the superposing of dynamic shear. On the other hand, Zhan et al.[21] found in an investigation of the film blowing process that the polymer melt strength increased when axial dynamic shear was superposed vertically to the flow direction.[21] Our previous work indicated that the melt strength is one of the most important parameters for microcellular foaming. Enhanced melt strength could improve the foamability of the polymer and the cellular structure of the ultimate foams.[22]

The purpose of this article is to present a way of performing PP microcellular foaming to achieve desired PP microcellular foams. The previous description shows that the shear and the melt strength are closely related to the microcellular foaming process. In this study, the dynamic shear induced by mechanical vibrations of a rotor was superposed on the microcellular foaming process to enhance the melt strength and foamability of PP. To determine the mechanism of the effects of dynamic shear on the foaming process, we theoretically analyzed the variations of the melt shear and melt strength with vibration parameters. In experiments, PP and HDPE were first blended to enhance the melt strength and improve the foamability.[23] PP/HDPE blends (70 : 30) were microcellularly foamed with different vibration parameters. Effects of static shear induced by rotor rotation and dynamic shear induced by axial vibration of the rotor on the microcellular structure of the foam were investigated in detail. In this study, supercritical CO_2 was used as the foaming agent. Supercritical CO_2 is one of the supercritical fluids characterized by a temperature higher than 31°C and a gas pressure higher than 7.37 MPa.[24] It is known that supercritical fluids have low viscosities and nearly zero surface tension; this allows fast mass transfer in the swollen polymer.[25] SO CO_2 has good solubility and diffusibility for many polymers,[26] and this is beneficial for the microcellular foaming process.

THEORETICAL ANALYSIS

Mathematical model

A self-made dynamic simulation foaming setup was used in this study. Its foaming unit consisted mainly of a rotor and a foaming chamber, as shown in Figure 1. The flowing melt in the foaming chamber was simplified, as shown in Figure 2, according to the configuration of the chamber. The rotor, mounted in the center of the foaming melt, could not only circumferentially rotate around the Z axis but also vibrate along the Z axis.

To simplify the theoretical analysis, the melt flow configuration in the foaming chamber was transformed into the melt flow in two flats of infinite sizes, as shown in Figure 3. The lower flat was considered to be static, and the upper flat not only linearly moved with a constant velocity along the X axis but also periodically vibrated along the Z axis.

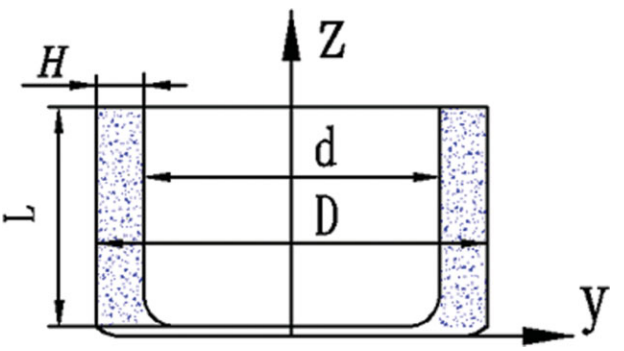

Figure 2 Schematic of the melt configuration in the foaming chamber. [Color figure can be viewed in the online issue, which is available at www.interscience.wiley.com.]

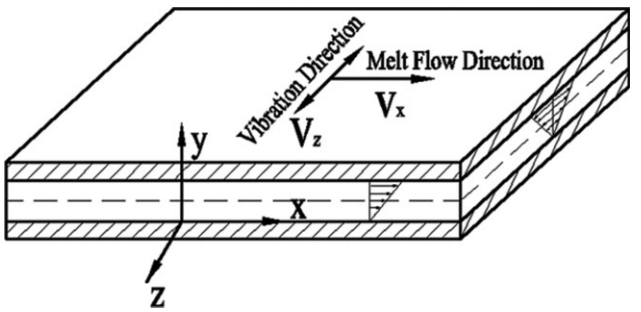

Figure 3 Physical model of the melt flow.

Assumptions

Before the theoretical analysis, the following assumptions were made:

1. The foaming melt is a steady and laminar flow.
2. The foaming solution fills the foaming chamber after the dissolution of supercritical CO_2 and does not flow out of the chamber.
3. The gravity and inertia effects can be ignored because of the highly viscous entangled polymer melt.
4. The polymer melt does not slip at the surface of the chamber.
5. The foaming process is considered to be isothermal.

Mathematical calculation and analysis

The linear motion of the upper flat is in the X direction with constant velocity u_0, as shown in Figure 3. The vibration of the upper flat is in the z direction with vibration amplitude A and vibration frequency f. The velocity of the upper flat can be expressed as follows:

$$V_x = u_0 \tag{1}$$

$$V_z = A\omega \cos \omega t \tag{2}$$

where V_x is the velocity of the upper flat in the flow or x direction, V_z is the velocity of the upper flat in the vibration or Z direction, t is the time, and ω is the angular frequency ($\omega = 2\pi f$).

On the basis of the previous assumptions, the melt velocity in the two flats is given by

$$v_{yx} = \frac{y}{H} u_0 \tag{3}$$

$$v_{yz} = \frac{y}{H} A\omega \cos \omega t \tag{4}$$

where y is the coordinate vertical to the x direction and z direction, v_{yx} is the melt velocity in the two flats in the x direction, v_{yz} is the melt velocity in the two flats in the z direction, and H is the distance of the two flats.

The melt shear rates between the two flats are

$$\dot{\gamma}_{yx} = \frac{u_0}{H} \tag{5}$$

$$\dot{\gamma}_{yz} = \frac{A}{H} \omega \cos \omega t \tag{6}$$

where $\dot{\gamma}_{yx}$ is the static shear rate induced by the rotor rotation in the x direction and $\dot{\gamma}_{yz}$ is the dynamic shear rate induced by the rotor vibration in the z direction.

Integrating the dynamic shear rate with the static shear rate results in a multiple-shear rate ($\dot{\gamma}$):

$$\dot{\gamma} = \sqrt{\dot{\gamma}_0^2 + (\gamma\omega \cos \omega t)^2} = \sqrt{\dot{\gamma}_0^2 + \left(\frac{A}{H} \omega \cos \omega t\right)^2} \tag{7}$$

where $\dot{\gamma}_0 = \dot{\gamma}_{yx} = u_0/H$.

Averaging $\dot{\gamma}$ in one period results in the average shear rate ($\overline{\dot{\gamma}}$):

$$\overline{\dot{\gamma}} = \sqrt{\frac{1}{T}\int_t^{t+T} \dot{\gamma}^2 dt} = \sqrt{\frac{1}{T}\int_t^{t+T} \left[\dot{\gamma}_0^2 + \left(\frac{A}{H} \omega \cos \omega t\right)^2\right] dt}$$

$$= \sqrt{\dot{\gamma}_0^2 + \frac{1}{2}\left(\frac{A\omega}{H}\right)^2} \tag{8}$$

where T is the vibration period.

Muke et al.[27] provided the relationship of the melt shear rate and the melt strength on the basis of experimental results:

$$\text{Melt strength} = k \exp(B\dot{\gamma}_a) \tag{9}$$

where k is the zero-shear melt strength (cN), B is the rising slope influencing the increase in the melt strength, and $\dot{\gamma}_a$ is the apparent shear rate.

The apparent shear rate has a direct relationship with the flow rate. The flow rate in the flow direction increases with an increase in the screw rotation speed. Muke et al.[27] reported that the increased melt flow rate was believed to result in a greater degree of built-in stresses in the melt, which led to the enhancement of the melt strength. In this study, the dynamic shear induced by the axial vibration of the rotor was vertically superposed on the static shear in the flow direction, and multiple shears were formed. The dynamic shear led to the increase in the shear rate, which resulted in an enhancement of the degree of built-in stresses and melt strength. On the other hand, the static shear and dynamic shear caused the molecular chains to align along two directions and cross each other. Then, a netting structure occurred in the polymer melt because of the entanglement of the molecular chains, which also led to the enhancement of the melt strength.[28]

On the basis of eq. (9) and previous experimental results, the relationships between the melt strength and vibration parameters produced the following:

$$\text{Melt strength} = k\exp\left((1.195)^{\frac{5}{3}A_0 f} B_0 \dot{\gamma}\right) \quad (10)$$

$$\text{Melt strength} = k\exp\left(1.26^{\frac{5}{3}Af_0} B_0 \dot{\gamma}\right) \quad (11)$$

where B_0 is the rising slope with no vibration, A_0 is a constant vibration amplitude, and f_0 is a constant vibration frequency. Equation (10) is the relation of the melt strength, shear rate, and vibration frequency. Equation (11) is the relation of the melt strength, shear rate, and vibration amplitude.

Parameter values (Table I)

Values of u_0 and H

$$u_0 = \frac{n\pi d}{60} \quad (12)$$

$$H = \frac{(D-d)}{2} \quad (13)$$

where D and d are the outer radius and inner radius of the polymer melt, respectively, and n is the rotation speed of the rotor.

Value of B

Melt strengths of PP (polypropylene) HDPE blends at different shear rates were measured on a high-pressure rheometer. The barrel diameter (D_1) of the rheometer was 15 mm, the die diameter (D_2) was 1 mm, and the die length (L) was 30 mm. The melting temperature was 180°C, the melt extrusion acceleration was 2 mm/s^2, and the initial extrusion velocity was 1.17 mm/s.

The melt apparent shear rate in the die can be expressed as follows:[29]

TABLE I
Basic Values of the Parameters

Parameter	Definition of the parameter	Value
u_0	Constant	76.6 mm/s
H	Distance of the two flats	1 mm
B_0	Rising slope with no vibration	0.006
k	Zero-shear melt strength	1.38
n	Rotation speed of the rotor	65 rpm
D	Outer radius of the polymer in the foaming chamber	24.5 mm
d	Inner radius of the polymer in the foaming chamber	22.5 mm
D_1	Barrel diameter of the rheometer	15 mm
D_2	Die diameter of the rheometer	1 mm

TABLE II
Values of the Apparent Shear Rate and Melt Strength with Various Downward Speeds of the Pillar

Downward speed of the pillar (mm/s)	Apparent shear rate (s^{-1})	Melt strength (cN)
0.075	135	3.85
0.1	180	5.83
0.25	450	13.2

$$\dot{\gamma}_a = \frac{8D_1^2 \cdot V_1}{D_2^3} \quad (14)$$

where V_1 is the downward speed of the pillar.

The melt strengths at different shear rates measured on the high-pressure rheometer are listed in Table II.

The values of B_0 and k can be obtained by the substitution of the data in Table II into eq. (9):

$$B_0 = 0.006, k = 1.38 \quad (15)$$

Theoretical results and discussion

Effects of the vibration frequency and amplitude on the shear rate

Figures 4 and 5 show the effects of the vibration frequency and amplitude on the apparent shear rate, respectively. As the vibration frequency and amplitude increase, the dynamic shear rate in the vertical direction of the flowing melt increases, and this leads to the increase in the melt apparent shear rate, as shown in Figures 4 and 5.

Effects of the dynamic shear on the melt strength

The melt strength is closely related to the shear rate. Increasing the shear rate leads to an enhancement of

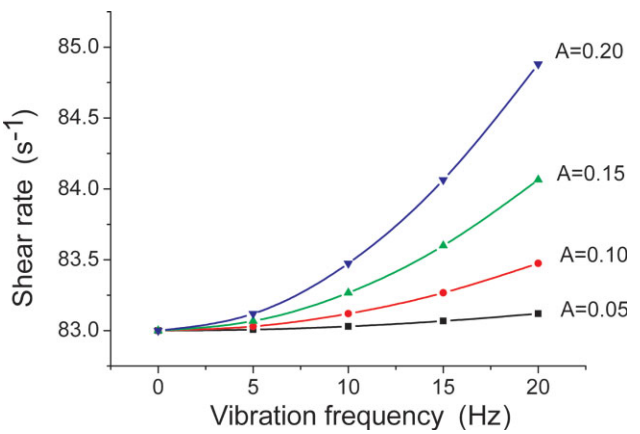

Figure 4 Effect of the vibration frequency on the shear rate (A = vibration amplitude). [Color figure can be viewed in the online issue, which is available at www.interscience.wiley.com.]

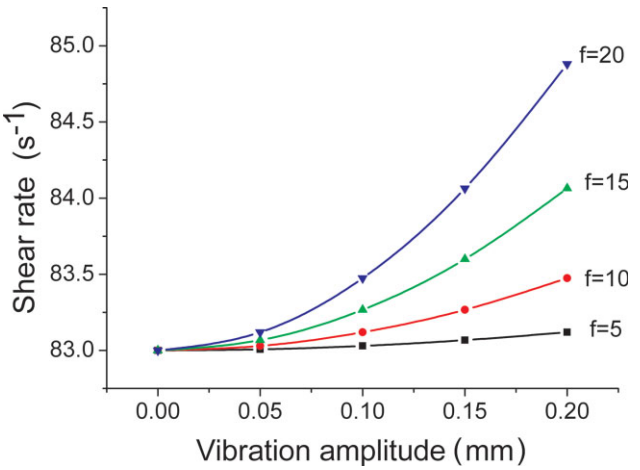

Figure 5 Effect of the vibration amplitude on the shear rate (f = vibration frequency). [Color figure can be viewed in the online issue, which is available at www.interscience.wiley.com.]

the melt strength because a higher shear rate results in a greater degree of built-in stresses in the melt.[27] The increase in these stresses requires a greater stretching force to extend the molecules and then leads to a higher melt strength. On the other hand, Han[30] reported that PP has a converging flow pattern in the entrance region of a capillary die. The converging flow results in an increase in the melt flow rate, and then linear melt stretching occurs. The molecular chains align along the linear stretching direction, and a regular molecular structure occurs. Then, the melt elasticity increases, and this leads to the increase in the melt strength.[31] The dynamic shear induced by the rotor vibration was superposed in this study. The melt shear rate increases as the vibration frequency and amplitude increase, as shown in Figures 4 and 5. It is obvious from Figures

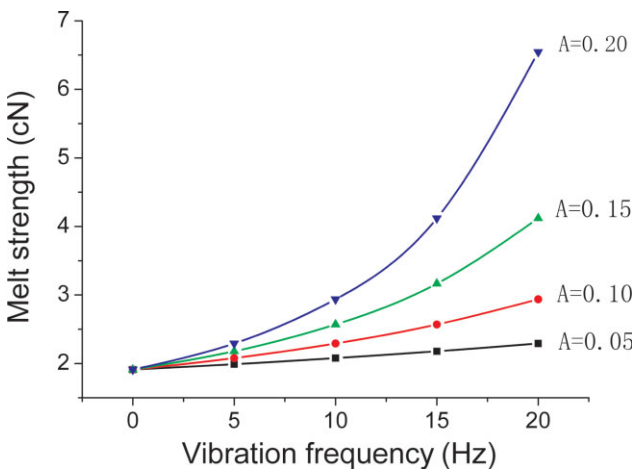

Figure 6 Effect of the vibration frequency on the melt strength (A = vibration amplitude). [Color figure can be viewed in the online issue, which is available at www.interscience.wiley.com.]

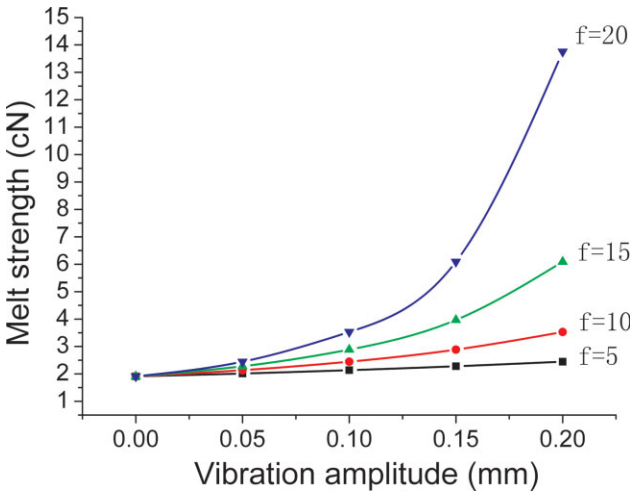

Figure 7 Effect of the vibration amplitude on the melt strength (f = vibration frequency). [Color figure can be viewed in the online issue, which is available at www.interscience.wiley.com.]

6 and 7 that a higher shear rate leads to an enhancement of the melt strength because of its close relationship with the melt strength. Furthermore, the dynamic shear induced by axial vibration is vertical to the static shear induced by rotor rotation. Then, the molecular chains align along two directions, and a netting structure forms; this leads to an increase in the entanglement of the molecular chains and a great enhancement of the melt strength, as shown in Figures 6 and 7.

EXPERIMENTAL

Materials

Copolymer PP and HDPE were used in this study. PP was supplied by Du Shan Zi Petrochemical Co. (Beijing, China) with a melt flow rate of 0.533 g/10 min (190°C, 2.16 kg). HDPE (5000S) was a

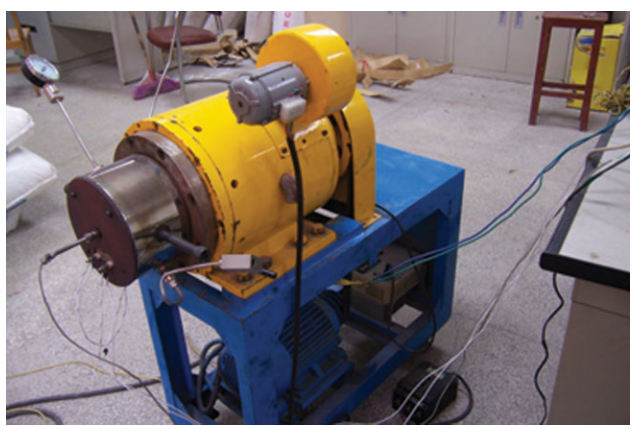

Figure 8 Dynamic simulation foaming setup. [Color figure can be viewed in the online issue, which is available at www.interscience.wiley.com.]

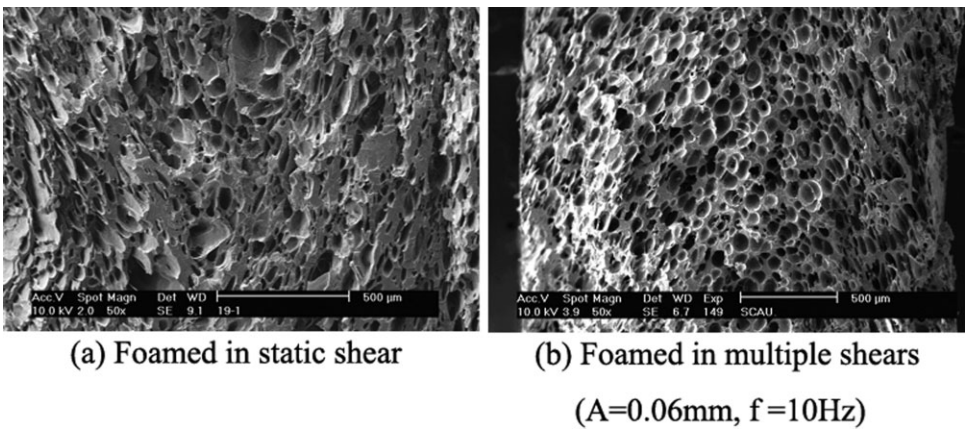

Figure 9 SEM micrographs of samples foamed in steady and multiple shears when the foaming temperature was 156°C (A = vibration amplitude and f = vibration frequency).

commercial product from Da Qing Petrol Chemical Co. (Daquing, China) with a melt flow rate of 0.533 g/10 min (190°C, 2.16 kg). HDPE (5000S) was a commercial product from Da Qing Petrol Chemical Co. with a melt flow rate of 0.9 g/10 min. Industrial liquid CO_2 with a purity of 99.5%, supplied by Guangzhou Jinzhu Chemistry Co., Ltd. (Guangzhou, China) was used as the foaming agent in this study.

Setup

A self-designed dynamic simulation foaming setup was used in this study, as shown in Figure 8. It mainly consisted of four parts: a self-made supercritical fluid supplier that could supply supercritical CO_2 with a maximum pressure of 25 MPa and a maximum volume of 15 L, a drive set, an electromagnetic dynamic device, and a foaming unit. The foaming unit mainly consisted of a rotor and a foaming chamber, as shown in Figure 1. The rotor could circumferentially rotate, driven by the drive set, and axially vibrate, driven by the electromagnetic dynamic device; this caused steady and dynamic shear forces, respectively. Both steady and dynamic foaming experiments could be carried out with this dynamic simulation foaming setup. A scanning electron microscope (XL30, Philip, Amsterdam, Holland) was used to observe the cellular structure.

Procedure

PP/HDPE blends were shaped into ring-shaped samples similar in size to the foaming chamber with a plane sulfuration machine (QLB-25D/Q, First Rubber and Plastic Factory of Wuxi, Wuxi, China). Each ring-shaped sample was put into the foaming chamber and heated to 180°C. After equilibrium for 15 min, the rotor began to rotate and vibrate to agitate the sample, and simultaneously, supercritical CO_2 was injected into the foaming chamber to a set saturation pressure. A uniform polymer/gas solution formed after CO_2 dissolved and diffused into the polymer melt under the action of the shear force of the rotor. The rotor was stopped after rotating and vibrating for 5 min. Then, the melt pressure quickly dropped with the opening of a depressurization

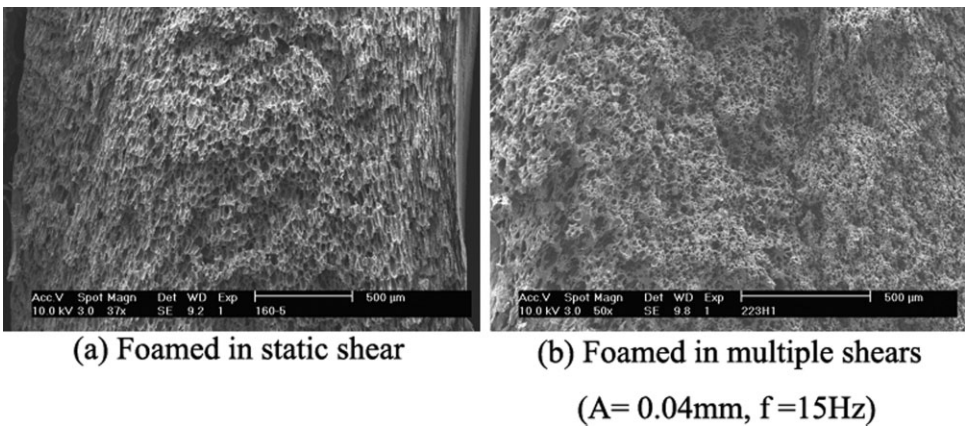

Figure 10 SEM micrographs of samples foamed in steady and multiple shears when the foaming temperature was 152°C (A = vibration amplitude and f = vibration frequency).

valve when the melt temperature reached the set foaming temperature via cooling of the chamber. The sudden depressurization of CO_2 in the polymer melt induced thermodynamic instability, and plenty of cells began to nucleate and grow. In the end, the cells were solidified via cooling with a fan (the cooling rate remained invariable in all experiments). The cellular structure of the ultimate foam was observed in scanning electron microscopy (SEM) pictures taken after cooling and breaking in liquid nitrogen.

RESULTS AND DISCUSSION

Effect of the dynamic shear on the cell distribution

PP/HDPE blends were foamed in static and multiple shears at different foaming temperatures. Figures 9 and 10 show SEM micrographs of samples foamed at 156 and 152°C, respectively. The cell size was enlarged and the cell density was reduced as the foaming temperature rose because of the decreases in the melt viscosity and melt strength. The cell density in the edge of the sample foamed in static shear was higher than that in the center, but the cell orientation in the foam edge was more severe, as shown in Figures 9(a) and 10(a). The reason is that the sample edge was nearer the rotor surface or the chamber inner wall, and this resulted in a higher shear rate. However, the higher shear rate in the sample edge produced a higher stretching force in the flow direction during cell growth, so the cell orientation was enhanced.

When the dynamic shear rate induced by the rotor vibration was superposed on the static shear rate, the multiple-shear rate that formed in the foaming fluid and the shear rate distribution became uniform; this led to a more uniform cell distribution and a decrease in the cell orientation. Furthermore, the dynamic shear rate was beneficial for the mixing of the CO_2/polymer solution and cell nucleation; this caused the increase in the cell density and the uniformity of the cell distribution, as shown in Figures 9(b) and 10(b).

Effect of the dynamic shear on the microcellular structure

Figure 11 shows SEM micrographs of ultimate foams with different vibration parameters in the flow direction and vertical direction. When the vibration was zero, the cell was drawn by the shear force, and then cell orientation occurred along the flow direction; this caused the cell diameter to be longer in the flow direction than in the vertical direction, as shown in Figure 11(a). Figure 11(b–f) shows that the cell orientation decreased and the cell became rounder as the vibration frequency and amplitude increased. This mainly occurred because the static shear and the dynamic shear were superposed and

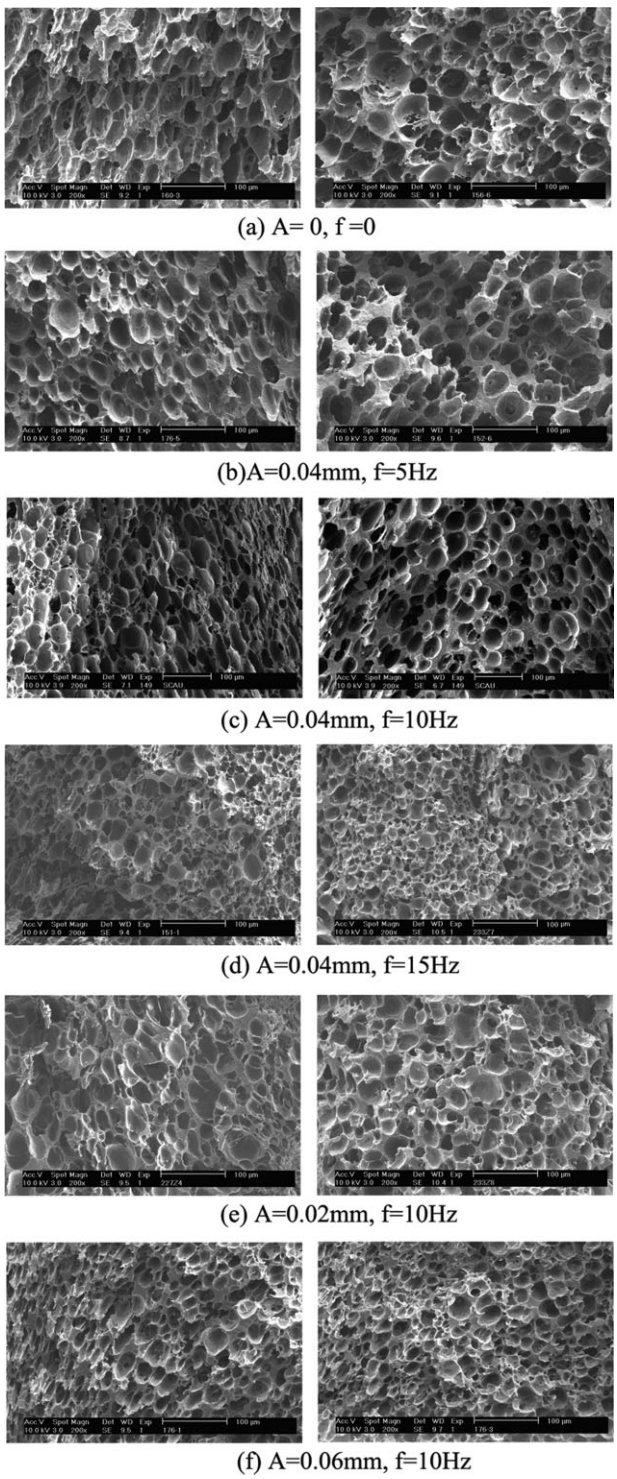

Figure 11 SEM photographs of microcellular foam samples with various vibration parameters (A = vibration amplitude and f = vibration frequency). The images on the left show the section in the flow direction, and the images on the right show the section vertical to the flow direction (temperature = 152°C, pressure = 12 MPa, rotation speed of the rotor = 65 rpm).

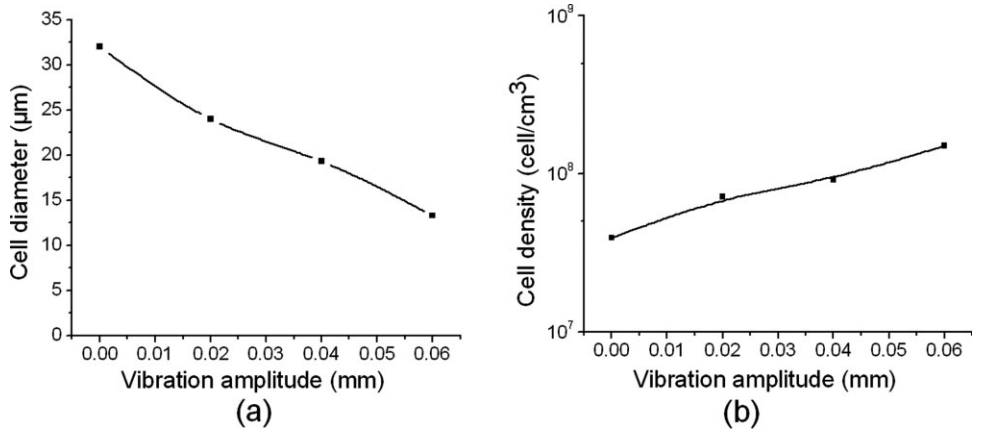

Figure 12 Effect of the vibration amplitude on (a) the cell diameter and (b) the cell density (vibration frequency = 10 Hz).

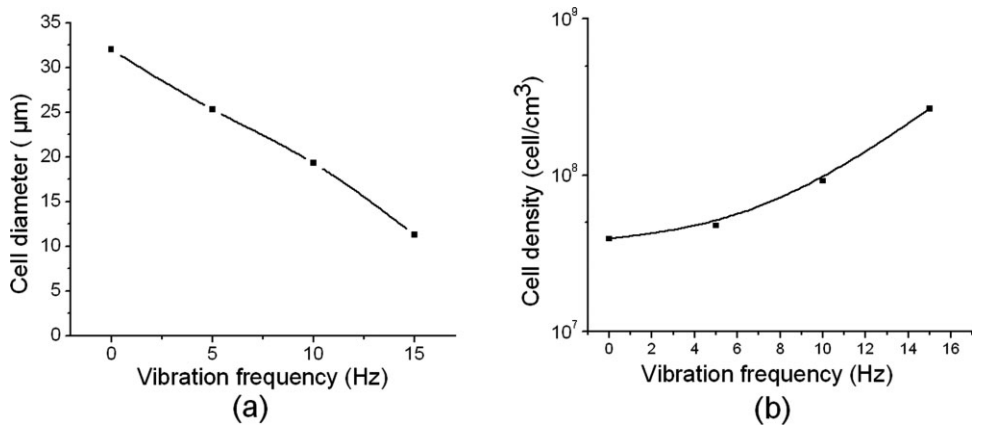

Figure 13 Effect of the vibration frequency on (a) the cell diameter and (b) the cell density (vibration amplitude = 0.04 mm).

the cell stretched along both directions; this led to the decrease in the cell orientation.

Figures 12 and 13 show the cell density and cell size as a function of vibration parameters based on Figure 11. Figures 4–7 indicate that the melt shear rate increased as the vibration frequency and amplitude increased, and this led to the enhancement of the melt strength. Higher melt strength effectively stabilized and restrained cell growth.[31] Therefore, the cell diameter decreased as the vibration amplitude and frequency increased, as shown in Figures 12(a) and 13(a). On the other hand, a higher shear rate enhanced the mixing of the polymer and CO_2, shortened the time of formation for the polymer/gas solution, and decreased the melt viscosity; this resulted in more cells to nucleate. Therefore, the cell density increased as the vibration frequency and amplitude increased, as shown in Figures 12(b) and 13(b). The smallest diameter was near 10 μm, and the highest density was about 2.66×10^8 cells/cm^3 at the vibration amplitude of 0.04 mm and at the frequency of 15 Hz. A comparison of Figures 12 and 13 indicated that the effect of the frequency on the cell structure was more than that of the amplitude.

CONCLUSIONS

A dynamic shear induced by rotor vibration was vertically superposed on the static shear, and its effects on the microcellular foaming of PP/HDPE blends were investigated theoretically and experimentally in this study. The theoretical analysis showed that the melt shear rate increased and the melt strength increased as the vibration frequency and amplitude increased. The experimental results showed that the cell had an elliptical shape, with the longer radius aligning along the melt flow direction when no vibration was superposed. Furthermore, the cell density in the sample edge was higher than that in the center, but the cell orientation in the sample edge was more severe because of the higher shear rate in the edge. The cell density increased, the cell size decreased, and the cell shape became rounder as the vibration frequency and amplitude

increased because of the increase in the melt shear rate and melt strength. The theoretical analysis was consistent with the experimental results. This study indicates that dynamic shear induced by axial vibration vertically to the flow direction can effectively enhance the melt strength and improve the foamability, and this is beneficial for PP microcellular foaming.

NOMENCLATURE

$\dot{\gamma}$	multiple-shear rate
$\overline{\dot{\gamma}}$	average shear rate in one vibration period
$\dot{\gamma}_a$	apparent shear rate
$\dot{\gamma}_{yx}$	static shear rate in the x direction
$\dot{\gamma}_{yz}$	dynamic shear rate in the z direction
ω	angular frequency
A	vibration amplitude
A_0	constant vibration amplitude
B	rising slope
B_0	rising slope with no vibration
d	inner radius of the polymer in the foaming chamber
CO_2	carbon dioxide
D	outer radius of the polymer in the foaming chamber
D_1	barrel diameter of the rheometer
D_2	die diameter of the rheometer
f	vibration frequency
f_0	constant vibration frequency
H	distance of the two flats
HDPE	high-density polyethylene
k	zero-shear melt strength
L	die length
n	rotation speed of the rotor
u_0	constant
PP	polypropylene
SEM	scanning electron microscopy
t	time
T	vibration period
V_1	downward speed of the pillar
V_x	velocity of the upper flat in the x direction
v_{yx}	melt velocity in the two flats in the x direction
v_{yz}	melt velocity in the two flats in the z direction
V_z	velocity of the upper flat in the z direction

References

1. Chen, L.; Wang, X.; Straff, R.; Chen, L.; Wang, X.; Rich, S.; Kent, B. Polym Eng Sci 2002, 42, 1151.
2. Nakajima, Y.; Kimura, T.; Nagaoka, Y. Eur. Pat. 0287011 B1 (1988).
3. Kimura, T.; Nagaoka, Y. U.S. Pat. 4,552,708 (1985).
4. Baldwin, D. F.; Park, C. B.; Suh, N. P.Polym Eng Sci 1998, 38, 674.
5. Lee, C. H.; Lee, K. J.; Jeong, H. G.; Kim, S. W. Adv Polym Technol 2000, 19, 97.
6. Doroudiani, S.; Park, C. B.; Kortschot, M. T. Polym Eng Sci 1996, 36, 2645.
7. Doroudiani, S.; Park, C. B.; Kortschot, M. T. Polym Eng Sci 1998, 38, 1205.
8. Rachtanapun, P.; Selke, S. E. M.; Matuana, L. M. J Appl Polym Sci 2003, 88, 2842.
9. Rachtanapun, P.; Selke, S. E. M.; Matuana, L. M. J Appl Polym Sci 2004, 93, 364.
10. Rachtanapun, P.; Selke, S. E. M.; Matuana, L. M. Polym Eng Sci 2004, 44, 1551.
11. Byon, S. K.; Youn, J. R. Polym Eng Sci 1990, 30, 147.
12. Cho, W. J.; Park, H.; Youn, J. R. Presented at the Winter Annual Meeting of the American Society of Mechanical Engineers, Anaheim, CA, 1992.
13. Cho, W. J.; Park, H.; Youn, J. R. Proc Inst Mech Eng B 1994, 208, 121.
14. Park, H.; Youn, J. R. Proc Int Mech Eng Cong Exposition 1994, p 125–137.
15. Baldwin, D. F.; Park, C. B.; Suh, N. P. Proc ASME Int Mech Eng Cong Exposition 1995, p 267–277.
16. Youn, J. R.; Park, H. Polym Eng Sci 1999, 39, 457.
17. Zhu, W. Doctoral Dissertation; South China University of Technology, 2005; p 78.
18. Zhou, N.; Zhu, W.; Peng, X. China Plast 2004, 18, 63.
19. Gao, C.; Zhou, N.; He, D. J Appl Polym Sci 2004, 32, 25.
20. Gao, C. Doctoral Dissertation, South China University of Technology, 2005; p 78.
21. Zhan, G. R.; Zhou, N. Q.; Peng, X. F. China Plast 2003, 17, 79.
22. Zhang, P.; Zhou, N. Q.; Wu., Q. F. J Appl Polym Sci 2007, 104, 4149.
23. Zhang, P.; Zhou, N.; Li, B.; Cao, X.; Wang, M. China Plast 2007, 2, 59.
24. Kazarian, S. G. Polym Sci 2000, 42, 78.
25. Li, D.; Liu, Z.; Han, B.; Song, L.; Yang, G.; Jiang, T. Polymer 2002, 43, 5363.
26. Nalawade, S. P.; Picchioni, F.; Janssen, L. P. B. M.; Patil, V. E. Polym Eng Sci 2006, 46, 643.
27. Muke, S.; Ivanov, I.; Kao, N.; Bhattacharya, S. N. Polym Int 2001, 50, 515.
28. Zhou, N. Q.; Zhang, P.; Wu, H. W.; Peng, X. F. J Appl Polym Sci 2006, 101, 83.
29. Xu, P. Rheology of the High Polymer and Its Application; Chemical Industry: Beijing, 2003.
30. Han, C. D. Rheology in Polymer Processing. Academic Press: New York, 1976.
31. Lau, H. C.; Bhattacharya, S. N.; Field, G. J. Polym Eng Sci 1998, 38, 1915.
32. Zhang, P.; Zhou, N. Q.; Wu, Q. F. J Appl Polym Sci 2007, 104, 4149.